Coherent chaos in a recurrent neural network with structured connectivity

Itamar Daniel Landau[1] and Haim Sompolinsky[1,2]

[1]Edmond and Lily Safra Center for Brain Sciences, Hebrew University of Jerusalem

[2]Center for Brain Science, Harvard University

Abstract

We present a simple model for coherent, spatially correlated chaos in a recurrent neural network. Networks of randomly connected neurons are known to exhibit chaotic fluctuations and have been studied as a model for the temporal variability of neocortical activity. The dynamics generated by such networks, however, are spatially uncorrelated and do not generate coherent fluctuations, which are commonly observed across spatial scales of the neocortex. In our model we introduce a structured component of connectivity, in addition to random connections, which effectively embeds a feedforward structure via unidirectional coupling between a pair of orthogonal modes. Local fluctuations driven by the random connectivity are summed by an output mode and drive coherent activity along an input mode. The orthogonality between input and output mode preserves chaotic fluctuations even as coherence develops. In the regime of weak structured connectivity we apply a perturbative approach to solve the dynamic mean-field equations, showing that in this regime coherent fluctuations are driven passively by the chaos of local residual fluctuations. Strikingly, the chaotic dynamics are not subdued by even very strong structured connectivity as long as we add a detailed balance constraint on the random connectivity. In this regime the system displays longer time-scales and switching-like activity reminiscent of "Up-Down" states observed in cortical circuits. The level of coherence grows with increasing strength of structured connectivity until the dynamics are almost entirely constrained to a single spatial mode. We describe how in this regime the network achieves intermittent self-organized criticality in which the coherent component of the dynamics self-adjusts to yield periods of slow chaos. Furthermore, we show how the dynamics depend qualitatively on the particular realization of the connectivity matrix: a complex leading eigenvector can yield coherent oscillatory chaotic fluctuations while a real leading eigenvector can yield chaos with broken symmetry. We examine the effects of network-size scaling and show that these results are not finite-size effects. Finally, we show that in the regime of weak structured connectivity, coherent chaos emerges also for a generalized structured connectivity with multiple input-output modes.

Introduction

Firing-rate fluctuations and irregular spiking are ubiquitous in the neocortex[23, 2]. Furthermore this temporal variability is often observed to be correlated across spatial scales ranging from local cortical circuits to the entire brain: in local cortical circuits both in membrane potential fluctuations [31] and on the level of spiking [22, 3, 15, 16], in the coherency measured in brain-wide EEG signals [14, 1], and in the global signal observed across all voxels in fMRI measurements [21, 10, 13].

A class of theoretical models has successfully accounted for temporal variability via internally generated chaotic dynamics of recurrent networks, whether through excitation-inhibition balance in spiking models[30, 18] or the more abstract models of rate chaos in randomly connected networks[24]. Yet a key emergent feature of these models is the decorrelation of neural activity such that the macroscopic, population activity remains nearly constant in time. Population-wide coherence or synchrony can be generated in a variety of ways for example by introducing spatial modes with self-excitation, but this comes at a cost of drowning out the chaotic fluctuations and yielding fixed points [28]. Indeed a major challenge to theorists has been to produce network models which generate spatially coherent, temporally irregular fluctuations which can account for broad spatial correlations observed in experiments.

Two recent studies have shown that excitation-inhibition balance networks can generate spatially modulated correlations [20, 5]. In both of these studies the correlations are driven by common input from an external source, and the average correlation across the network remains small. It remains an open question whether a network can internally generate correlated fluctuations that are coherent across the entire network.

The chaotic dynamics of a network of randomly connected firing-rate neurons has been well-studied [24, 9]. In such a network each individual neuron's firing rate is given by a non-linear function of its input, which is in turn a weighted sum of the firing rates of all other neurons in the network. The network exhibits a phase transition from a fixed point to chaotic activity in which the randomness of the weights reverberates uncorrelated fluctuations throughout the network. Typically in this chaotic regime pairwise correlations are small and no coherent fluctuations emerge. Here we extend this model by adding a low-rank structured component of connectivity to the random connections. The structured connectivity sums the fluctuations along one spatial mode and projects them along a second, orthogonal mode yielding coherent fluctuations without drowning out the individual neuron variability which continues to drive the chaotic dynamics. A previous work studied a specific example of this structure and focused primarily on analyzing the non-chaotic regime[6]. Here we focus on the chaotic regime and show that this form of structured connectivity together with random connections provides a basic mechanism for internally generating coherent fluctuations.

Results

We study a network of N neurons in which the connectivity between neurons has two components: a random component, $\mathbf{J}$, and a rank-1 structured component, $\mathbf{M} = \frac{J_1}{\sqrt{N}}\boldsymbol{\xi}\boldsymbol{\nu}^T$, an outer product of a pair of orthogonal vectors both of which have elements of $O(1)$ and norm $\sqrt{N}$, with strength parameter J_1. We restrict the elements of $\boldsymbol{\xi}$ to be binary, $\xi_i = \pm 1$, which will be important for some of the results to come, and we will comment on when this restriction can be relaxed. We can think of the row vector, $\boldsymbol{\nu}^T$, as an "output mode" performing a read-out of the network activity, and the column vector, $\boldsymbol{\xi}$, as a corresponding "input mode" along which the output mode activity is fed back to the network. (Fig 1A) .

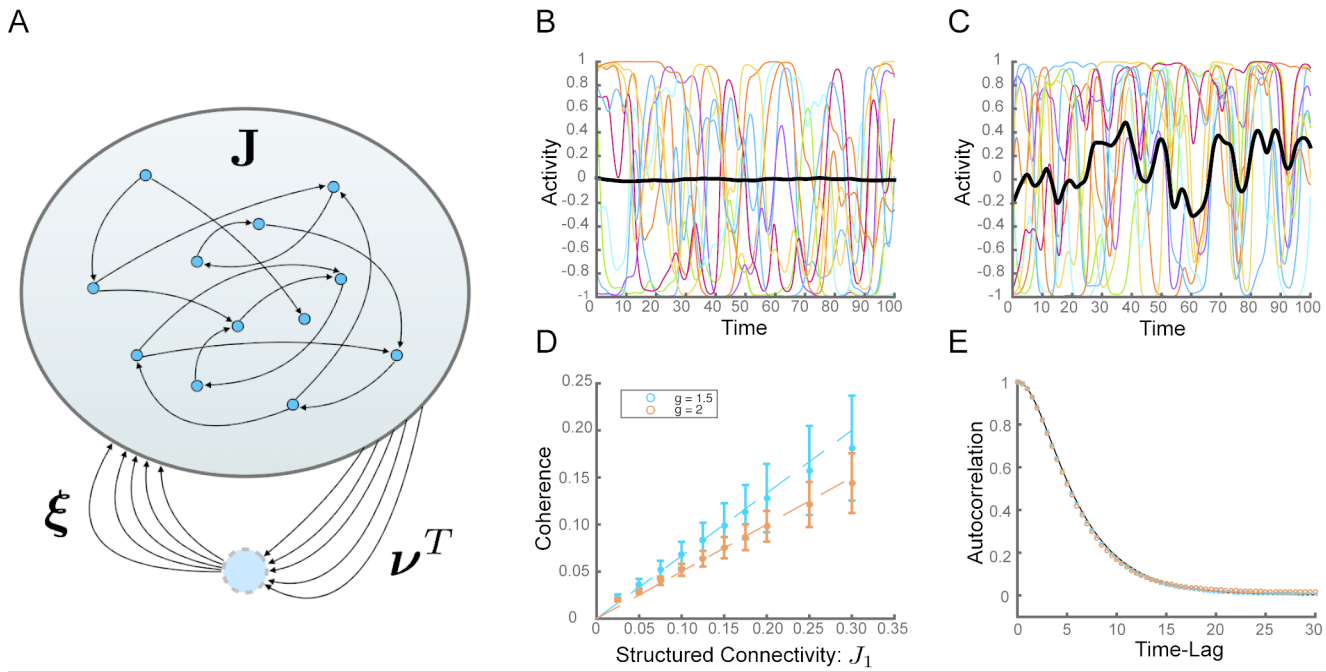

Figure 1. Weak Structured Connectivity Generates Passive Coherence. **(A)** Network schematics showing neurons connected via random matrix $\mathbf{J}$ and rank-one structured connectivity. The structured component is represented schematically as a feed-forward loop with drive through the output mode, $\boldsymbol{\nu}$, and feedback through the input mode, $\boldsymbol{\xi}$. The standard deviation of the random component is given by $\frac{g}{\sqrt{N}}$ and the strength of the structured component is $\frac{J_1}{\sqrt{N}}$. **(B)** Sample network dynamics without structured component, i.e. $J_1 = 0$, colored traces show a random collection of ten neural activity patterns, ϕ_j, black trace shows the coherent mode activity, $\bar{\phi} = \frac{1}{N}\sum_j \xi_j \phi_j$. **(C)** Sample dynamics for $J_1 = 1$. Coherent mode displays substantial fluctuations. **(D)** Coherence χ (Expression in Text), as a function of the strength of structured connectivity component, J_1. Simulation and theory shown for both $g = 1.5$ and $g = 2$. Bars show standard deviation over 60 realization of the random connectivity. **(E)** Normalized autocorrelation of the coherent component of the current in red circles. Average normalized autocorrelation of the residuals in blue 'x's. Both are averaged over 60 realizations of the random connectivity with $g = 2$ and $J_1 = 0.1$. Prediction from theory in black. $N = 4000$ in all panels.

The random component of the connectivity is given by the matrix $\mathbf{J}$ consisting of identically distributed independent Gaussian elements with mean 0 and variance $\frac{g^2}{N}$, where g is an $O(1)$ parameter.

The state of each neuron is defined by its synaptic current, $h_i(t)$, with its firing rate given by $\phi_i \equiv \phi(h_i(t))$, where

ϕ is a sigmoidal function. For some later results it will be necessary to assume that ϕ has a first derivative that is an even function. We therefore assume here for concreteness $\phi(h) = \tanh(h)$ unless otherwise noted, and we comment on when this assumption can be relaxed.

The dynamics of the synaptic current vector, $\mathbf{h}$, is given by

$$\frac{\mathrm{d}\mathbf{h}}{\mathrm{d}t} = -\mathbf{h} + \mathbf{J}\boldsymbol{\phi} + \frac{J_1}{\sqrt{N}}\boldsymbol{\xi}\boldsymbol{\nu}^T\boldsymbol{\phi} \tag{1}$$

We have scaled the strength of the structured connectivity such that when the scaling-parameter $J_1 \sim O(1)$ the contribution of the structure to individual synapses is of the same order of magnitude as the typical random connection.

We will be particularly interested in the coherent activity and the coherent current, i.e. the spatial overlap of both the firing rate and the synaptic current with the input mode. These are defined respectively as

$$\bar{\phi} \equiv \frac{1}{N}\sum_j \xi_j \phi_j, \ \bar{h} \equiv \frac{1}{N}\sum_j \xi_j h_j, \tag{2}$$

We define the measure of coherence as the fraction of the total standard deviation of the network current h_i that is shared along the coherent mode, $\bar{h}$:

$$\chi \equiv \sqrt{\frac{\langle \bar{h}^2 \rangle}{\frac{1}{N}\sum_i \langle h_i^2 \rangle}} \tag{3}$$

where $\langle\ \rangle$ represents average over time. This is a useful measure as it varies from 0 to 1, and will yield $\chi = 1/\sqrt{N}$ for entirely independent, uncoupled fluctuations, and $\chi = 1$ for complete synchrony along $\boldsymbol{\xi}$.

Without the structured component, i.e. $J_1 = 0$, the network exhibits a phase transition at $g = 1$ from a zero fixed point to chaos[24]. In the chaotic state the randomness of the connectivity decorrelates the input current and yields an asynchronous state in which neurons fluctuate with negligible correlations such that both $\bar{\phi}$ and $\bar{h}$ are nearly constant in time, and $\chi \approx \frac{1}{\sqrt{N}}$ (Fig 1B).

Setting $J_1 = 1$, we observe significant correlations along the input mode, such that the coherent mode activity, $\bar{\phi}$, fluctuates significantly. For this network with $N = 4000$ we find the coherence $\chi \approx 0.4$, which is about 25 times larger than is observed in the asynchronous state. (Fig 1C).

In order to analyze this system we decompose the dynamics of the synaptic currents into coherent component, $\bar{h}$, and the vector of residuals currents, $\delta\mathbf{h} = \mathbf{h} - \bar{h}\boldsymbol{\xi}$. We also decompose the activity into its coherent component, $\bar{\phi}$, and vector of residual activity, $\delta\boldsymbol{\phi} = \boldsymbol{\phi} - \bar{\phi}\boldsymbol{\xi}$. We note that because of the orthogonality between input and

output mode, the output mode ignores the coherent component, $\bar{\phi}$, and projects only the activity of the residuals: $\boldsymbol{\nu}^T \boldsymbol{\phi} = \boldsymbol{\nu}^T \delta\boldsymbol{\phi}$.

By averaging the dynamic equations 1 over the input mode, $\boldsymbol{\xi}$, we can decompose the dynamics of the residual synaptic currents from the dynamics of the coherent current:

$$\frac{\mathrm{d}\delta\mathbf{h}}{\mathrm{d}t} = -\delta\mathbf{h} + \mathbf{J}\boldsymbol{\phi} \tag{4}$$

$$\frac{\mathrm{d}\bar{h}}{\mathrm{d}t} = -\bar{h} + \frac{J_1}{\sqrt{N}}\boldsymbol{\nu}^T \delta\boldsymbol{\phi} \tag{5}$$

The full system includes the constraint that $\sum_j \xi_j \delta h_j = 0$ but we will attempt to approximate the system by ignoring the constraint and treating the coupled set of equations in $N+1$ dimensions. This approximation ignores the projection of the random component of the connectivity along the coherent mode. Note even in this approximation, the nonlinearity of ϕ in these equations, couples the coherent and residual degrees of freedom.

In order to attempt to solve the approximate system we can assume that $\bar{h}(t)$ fluctuates according to some known random process and then consider the dynamics of the δh_i with the firing rate of individual units as given by $\phi\left(\delta h_i(t) + \xi_i \bar{h}(t)\right)$. However, for general J_1 we are unable to analytically close the loop and self-consistently compute the statistics of $\bar{h}(t)$.

Mildly Coherent Chaos

In order to proceed analytically, we take a perturbative approach, assuming $J_1 \ll 1$. We turn to computing the autocorrelations of both the coherent component

$$\bar{\Delta}(\tau) \equiv \left\langle \bar{h}(t)\, \bar{h}(t+\tau) \right\rangle \tag{6}$$

and of the residuals,

$$\Delta_\delta(\tau) \equiv \left\langle \delta h_i(t)\, \delta h_i(t+\tau) \right\rangle \ . \tag{7}$$

For small J_1 we assume that the coherent activity $\bar{\phi} \ll 1$ and therefore in the dynamics of the residual currents 4 we approximate $\boldsymbol{\phi} \approx \delta\boldsymbol{\phi}$. The result is that to leading order the autocorrelation of the residuals is given by the zeroth-order ($J_1 = 0$) autocorrelation

$$\Delta_\delta(\tau) \approx \left\langle h_i(t)\, h_i(t+\tau) \right\rangle_{J_1=0} \tag{8}$$

That is, the residual inputs fluctuate as independent Gaussian processes almost identically to the situation without structured connectivity. These residual fluctuations are summed over the output mode yielding substantial fluctuations in $\boldsymbol{\nu}^T \delta\boldsymbol{\phi}$ (recall, $\nu_i \sim O(1)$). These in turn drive the coherent mode and we show in Methods its autocorrelation is given to first-order by

$$\bar{\Delta}(\tau) \approx \left(\frac{J_1}{g}\right)^2 \Delta_\delta(\tau) \tag{9}$$

This tells us that to leading order the autocorrelation of the coherent component is simply a scaled version of the local, residual autocorrelation.

We verify this prediction numerically in Fig 1E for $J_1 = 0.2$ showing the normalized autocorrelations, $q_{\bar{h}}(\tau) = \frac{\bar{\Delta}(\tau)}{\bar{\Delta}(0)}$ and $q_\delta(\tau) = \frac{\Delta_\delta(\tau)}{\Delta_\delta(0)}$ as well as the prediction from theory. Qualitatively this means that in this regime chaos is driven by the emergent fluctuations in the local synaptic current similar to in the $J_1 = 0$ case, and that the coherent component can be said to absorb these fluctuations passively along the input mode, $\boldsymbol{\xi}$.

In this regime the coherence is given simply by

$$\chi = \sqrt{\frac{\bar{\Delta}(0)}{\bar{\Delta}(0) + \Delta_\delta(0)}} \approx \frac{J_1}{g} \tag{10}$$

Numerically, we find that this approximation provides a good description of the system's state for up to $J_1/g = 0.1$.

We can understand the coherent chaos in this regime qualitatively: the residual synaptic currents driven by the random connectivity fluctuate as uncorrelated Gaussian processes, and the resulting independent fluctuations in firing rates will be summed over the output mode, $\boldsymbol{\nu}$, which projects to the input mode, $\boldsymbol{\xi}$, driving coherent fluctuations in $\bar{h}(t)$. If the two modes, $\boldsymbol{\xi}$ and $\boldsymbol{\nu}$ had substantial overlap then the coherent fluctuations along $\boldsymbol{\xi}$ would drive positive feedback through $\boldsymbol{\nu}$ driving the neurons to a fixed point. The orthogonality of these modes effectively embeds a feedforward structure from the output mode, $\boldsymbol{\nu}$, to the input mode, $\boldsymbol{\xi}$, within the recurrent connectivity. This enables the persistence of stable fluctuations along the input mode, $\boldsymbol{\xi}$, which do not feedback to $\boldsymbol{\nu}$, thus preventing either saturation or oscillations.

We note that in the regime of mild coherence we can relax the restrictions on $\boldsymbol{\xi}$ and ϕ. Our results here hold for any $\boldsymbol{\xi}$ which is norm $\sqrt{N}$ and orthogonal to $\boldsymbol{\nu}$, and for any smooth non-linearity.

Non-Self-Averaging and "Detailed Balance" Connectivity

We observe that as J_1 increases to values of $O(1)$, the network displays significant variability in the dynamics from realization to realization. In particular, the overall autocorrelation function is no longer self-averaging (Fig 2A).

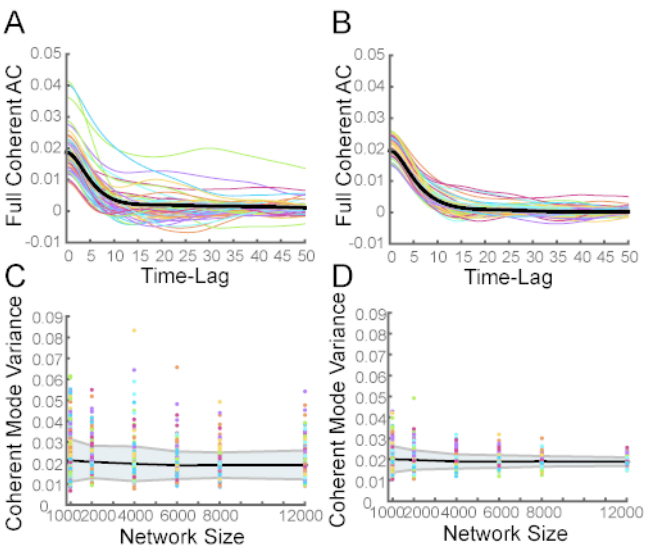

Figure 2. Detailed Balance Ensures Self-Averaging. (A)-(B) Full coherent mode autocorrelation, $\bar{\Delta}(\tau)$, of 60 individual realizations, $J_1 = 0.2$ and $N = 4000$. Thick black line shows average over realizations. **(A)** Network with random connectivity $\mathbf{J}$ without detailed balance. Significant difference between realizations **(B)** Network with "detailed balance" random connectivity, $\tilde{\mathbf{J}} = \mathbf{J} - \mathbf{J} \cdot \frac{1}{N}\left(\boldsymbol{\xi} \cdot \boldsymbol{\xi}^T\right)$. Individual realizations are all very close to the average. **(C)-(D)** Coherent mode variance, $\bar{\Delta}(0)$, as a function of network size for 300 individual realizations. Black line shows average and gray region shows standard deviation over realizations. **(C)** Without detailed balance standard deviation saturates. Variability between realizations is not a finite-size effect. **(D)** With detailed balance standard deviation shrinks, variability between realizations is a finite-size effect.

In the limit of small J_1 we were able to ignore the way the coherent activity is filtered through the random connectivity, $\mathbf{J}$. We can write the transformation of the input mode via the random connectivity as

$$\mathbf{J}\boldsymbol{\xi} = a_{\parallel}\boldsymbol{\xi} + \boldsymbol{\xi}^{\perp} \tag{11}$$

where $a_{\parallel}$ is a realization-dependent scalar and $\boldsymbol{\xi}^{\perp}$ is a realization-dependent vector orthogonal to $\boldsymbol{\xi}$. As J_1 increases and the fluctuations in the coherent activity along the input mode increase this transformation becomes more significant in a number of ways. First of all, the random connectivity maps the coherent activity back along the input mode with realization-dependent component, $a_{\parallel}$, and therefore the coherent activity, $\bar{\phi}$, drives feedback directly to the coherent current $\bar{h}$:

$$\frac{\mathrm{d}\bar{h}}{\mathrm{d}t} = -\bar{h} + J_1 \boldsymbol{\nu}^T \cdot \delta\boldsymbol{\phi} + a_{\parallel}\bar{\phi}$$

Secondly, the random connectivity maps the coherent activity in a realization-dependent direction, $\boldsymbol{\xi}^{\perp}$, so that $\bar{\phi}$ drives the residual activity fluctuations $\delta\boldsymbol{\phi}$ along this direction. This direction will have realization-dependent com-

ponent along the output mode, $\boldsymbol{\nu}$, and therefore the coherent activity may additionally drive feedback by pushing the residual fluctuations along the output mode.

To suppress the strong realization dependence of the dynamics, we refine the random connectivity matrix by defining

$$\tilde{\mathbf{J}} \equiv \mathbf{J} - \mathbf{J} \cdot \frac{1}{N} \left(\boldsymbol{\xi} \cdot \boldsymbol{\xi}^T \right) \tag{12}$$

This "detailed balance" subtraction has been previously observed to remove realization-dependent outliers from the eigenspectrum of the full connectivity matrix [17, 27]. Here we observe that detailed balance guarantees that our decomposition into residual and coherent dynamics in Eqns 4 and 5 is exact (together with the constraint $\sum_j \xi_j \delta h_j = 0$).

Furthermore, we find here that detailed balance suppresses realization-to-realization variability in the nonlinear chaotic dynamics. The detailed balance yields self-averaging, reducing the variability in the full autocorrelation of the coherent mode between individual realizations (Fig 2B). Furthermore, we observe that with detailed balance this variability drops as a function of increasing system size, whereas variability without detailed balance appears to remain large for large N.

The impact of detailed balance on the chaotic dynamics can be understood by noting that the resulting connectivity matrix, $\tilde{\mathbf{J}}$, now has a null-space, and the input mode, $\boldsymbol{\xi}$, lies within it. The result of detailed balance then is to ensure that the random connectivity matrix filters out any coherent activity fluctuations, $\bar{\phi}(t)$:

$$\tilde{\mathbf{J}}\boldsymbol{\phi} = \tilde{\mathbf{J}} \left(\bar{\phi}\boldsymbol{\xi} + \delta\boldsymbol{\phi} \right) = \tilde{\mathbf{J}}\delta\boldsymbol{\phi} \tag{13}$$

This prevents the coherent mode activity from driving feedback to the dynamics of the coherent current, either directly via $a_{\parallel}$ or through biasing the direction of residual fluctuations to $\boldsymbol{\xi}^{\perp}$.

Highly Coherent Chaos

What happens when the structured connectivity is made stronger? One would expect that as the dynamics became more coherent, very quickly the residual fluctuations would become entirely drowned out, because of the saturation nonlinearity of ϕ, so the system is no longer in the chaotic regime. Indeed, when sufficiently strong spatial coherence is induced by a symmetric connectivity, e.g., $J_1 \boldsymbol{\xi}\boldsymbol{\xi}^T/N$ the system exhibits a coherent fixed point for sufficiently large J_1 [28, 11]. Surprisingly, we find that with detailed balance, increasing J_1 yields chaotic dynamics which are strikingly coherent and display switching-like macroscopic activity (Fig 3A).

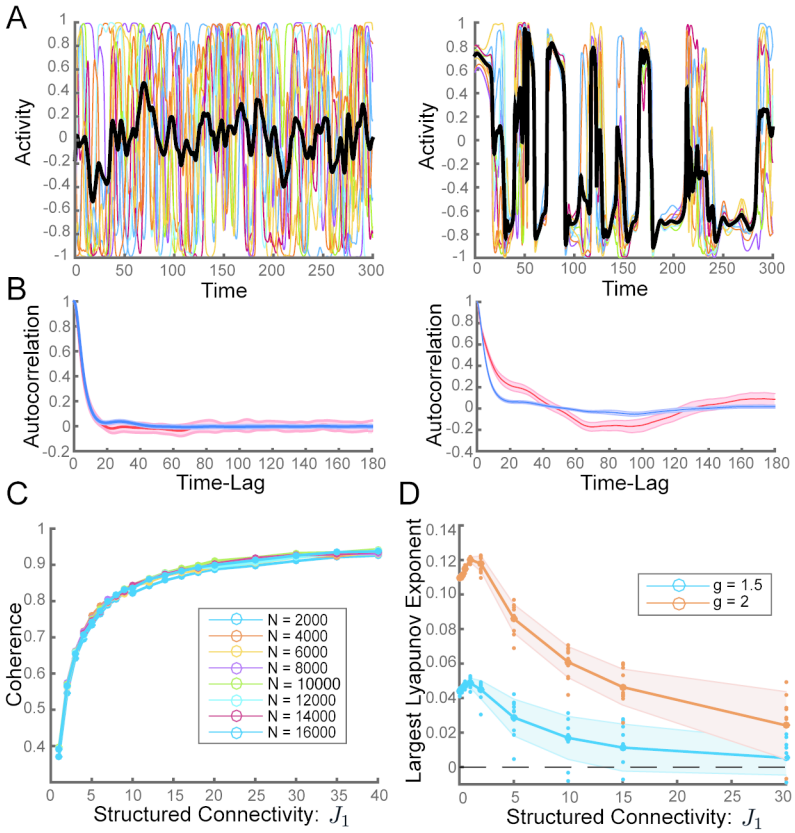

Figure 3. Strong Structured Connectivity Generates High Coherence Even as Chaos Persists. (A) Sample activity of 10 randomly chosen neurons, ϕ_j, and coherent mode activity, $\bar{\phi}$, in black. Strong structured connectivity yields chaotic activity that is highly coherent with switching-like behavior. **(B)** Normalized autocorrelation of coherent mode in red, and residual in blue. Shaded regions show standard deviation over 25 initial conditions of the same connectivity. Strong structured connectivity yields coherent mode dynamics which are independent of the residuals. **(A)-(B)** $N = 4000$ Left: $J_1 = 0.8$. Right: $J_1 = 15.8$. **(C)** Coherence, χ, as a function of J_1 for different network sizes exhibits universality. Coherence appears to approach 1 as J_1 is increases demonstrating that chaos persists even as fluctuations in the residuals shrink. Coherence is averaged over 30 realizations of the connectivity for each N, excluding the few fixed points and limit cycles that occur for larger J_1 (2 out of 30 or less for the largest values of N). **(D)** Largest Lyapunov exponent as a function of J_1. Thick line shows average over 10 realizations, small dots show values for individual realizations, and shaded region is standard deviation. All but a small fraction of realizations are chaotic, even in the region where $\chi > 0.9$. $g = 2$ in all panels unless noted otherwise

In contrast to the mild-coherence regime, in strong coherence the coherent mode dynamics are no longer passively driven by the fluctuations in the residual synaptic currents. This is evidenced by the normalized autocorrelation of the coherent mode, $\bar{q}(\tau)$, which is no longer close to the normalized residual autocorrelation, $q_\delta(\tau)$, but rather has qualitatively different dynamics including longer time-scales (Fig 3B).

We increase J_1 up to values of 100 and observe that chaos persists and coexists with a very high degree of spatial coherence. The coherence measure, χ, increases with increasing $J_1$and reaches values higher than 0.96 even as fluctuations persist (Fig 3C and Fig S1). We calculate the largest Lyapunov exponent and verify that the dynamics

are indeed chaotic for a vast majority of realizations even as the dynamics are highly coherent (Fig 3C).

Transition to low-dimensional dynamics for strong structured connections

We observe that for fixed system size and for each particular realization of the random connectivity, there is a value of J_1 above which the network reaches either a fixed point or a limit cycle. This result has been previously observed and analyzed [6].

Each realization exhibits a phase transition in the parameter space of J_1vs g, and the critical curve $J_1^c(g)$ is monotonically increasing. The shape and location of this curve are realization dependent. (Fig 4A-B)

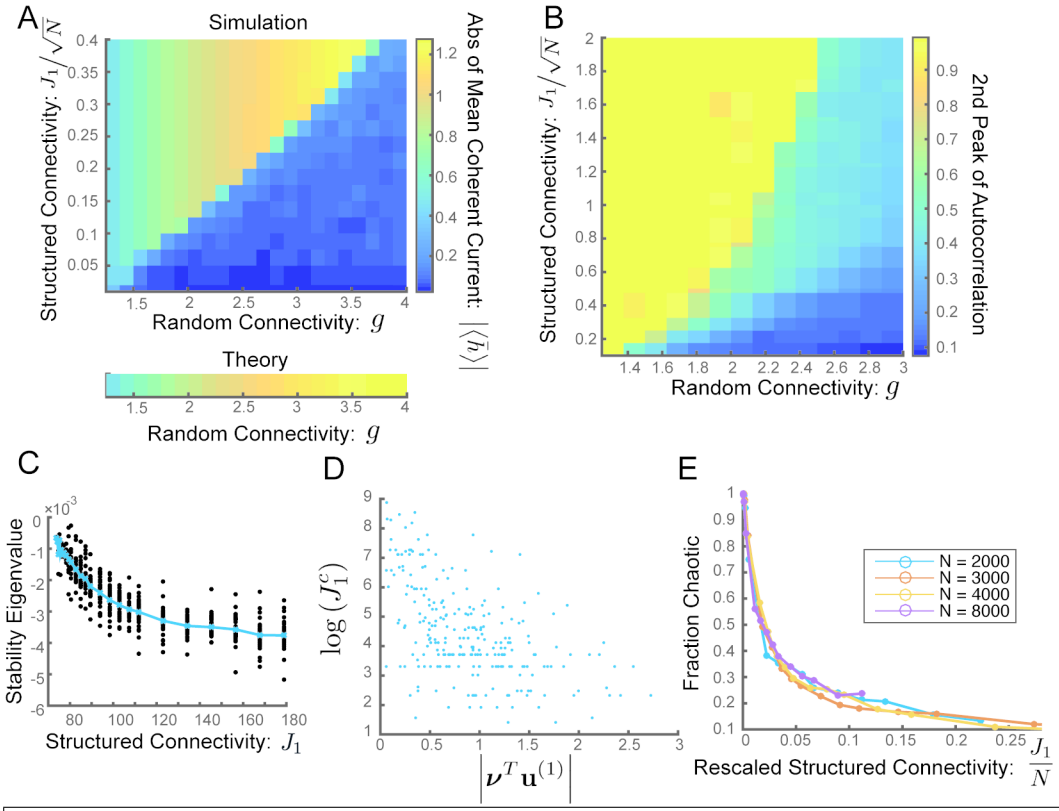

Figure 4. Sufficiently Strong Structure Yields Transition Out of Chaos: **(A)** Phase diagram for a single connectivity realization with real leading eigenvector. Colormaps the absolute value of the mean coherent current over a single trial, $|\langle\bar{h}\rangle|$ which is close to zero when the network is chaotic and non-zero when at a fixed point. **(B)** Phase diagram for a single connectivity realization with complex leading eigenvector. Colormap shows the second peak of the normalized autocorrelation of the coherent mode. This is 1 if the dynamics are perfectly oscillatory. $N = 4000$ for **(A)-(B)**. **(C)** Stability eigenvalue at fixed point, i.e. leading eigenvalue of the Jacobian, as a function of J_1 for a specific realization of the random connectivity. The fixed point exhibits marginal stability independent of J_1. **(D)** Scatterplot of the logarithm of transitional value of J_1 vs the absolute value of the projection of the output mode, $\boldsymbol{\nu}$, on the leading eigenvector, $\mathbf{u}^{(1)}$ for 300 connectivity realizations with $N = 8000$. $r^2 = 0.29$. **(E)** Fraction of realizations displaying chaotic activity as a function of the rescaled structured connectivity: $\frac{J_1}{N}$. With this scaling the curve appears to be independent of N.

As was previously shown[6], for a given realization of $\tilde{\mathbf{J}}$, for large enough J_1 the residual dynamics will be entirely contained in the subspace spanned by the leading eigenvector of $\tilde{\mathbf{J}}$. If this eigenvalue is real then the corresponding eigenvector is real and the resulting dynamics are a fixed point. If the leading eigenvalue is complex the resulting dynamics are a limit cycle. We review these analytical results and report further numerical evidence in Methods and Supplementary. Here we briefly discuss the case of a real leading eigenvalue, $\tilde{\mathbf{J}} \cdot \mathbf{u}^{(1)} = \lambda_1 \mathbf{u}^{(1)}$. A well known result from the theory of random matrices is that $\lambda_1 \approx g$.

In the regime where $J_1 \gg 1$, the residual synaptic currents are small, $\delta h_i \ll 1$, and we can approximate $\phi_j \approx \xi_j \phi\left(\bar{h}\right) + \phi'\left(\bar{h}\right) \delta h_j$. Assuming a fixed point value for the coherent mode, $\bar{h}^*$, the result is a set of fixed point equations for the residual synaptic currents (see Eq. 4 with $\tilde{\mathbf{J}}$):

$$\delta \mathbf{h}^* = \phi'\left(\bar{h}^*\right) \tilde{\mathbf{J}} \delta \mathbf{h}^* \tag{14}$$

implying that the vector of residuals is proportional to the leading eigenvector $\mathbf{u}^{(1)}$, i.e. $\delta \mathbf{h}^* = c_1 \mathbf{u}^{(1)}$, and additionally the coherent mode $\bar{h}^*$must be at the critical value at which

$$\phi'\left(\bar{h}^*\right) = \frac{1}{\lambda_1} \approx \frac{1}{g} \tag{15}$$

Substituting this value of $\bar{h}^*$ into the fixed point equation for the coherent mode (see Eq. 5) fixes the scale factor, c_1,

$$c_1 = \frac{\bar{h}^* g}{{}^{J_1}/\sqrt{N}\left(\boldsymbol{\nu}^T \mathbf{u}^{(1)}\right)} \tag{16}$$

We confirm numerically that this fixed point is reached above the critical curve $J_1^c\left(g\right)$, with $\left|\left\langle \bar{h}^* \right\rangle\right| \approx \phi'^{-1}\left(\frac{1}{g}\right)$ independent of the value of J_1(Fig 4A and Fig S2). Interestingly, this mechanism is reminiscent of self-organized criticality, namely the dynamics drive the system toward a a marginal fixed point, without fine tuning of stability parameter. Indeed, we confirm numerically (Fig 4C), that independent of J_1 the fixed point has very small stability-eigenvalue.

As we show in Methods, the case of complex leading eigenvalue for $\tilde{\mathbf{J}}$,the system converges to a limit cycle which also exhibits self-organized criticality. In that case the average slope of the transfer function $\phi'\left(\bar{h}\right)$ over each period is ${}^1/_g$ independent of J_1, and the frequency is given by the phase of the leading eigenvalue (SI Fig). The phase of the typical leading eigenvalue decreases with system size, and therefore the typical period of the limit cycle diverges as system size grows to infinity.

Notice the crucial role of detailed balance, without which a fixed point with small residuals is not at all possible (since the coherent component of the activity is not cancelled out to yield homogeneous fixed-point equations for the residuals, as in Eq. 14). Note also the role of the binary structure of $\xi_j = \pm 1$ and the symmetry of the transfer function, which together yield $\phi(\xi_j x) = \xi_j \phi(x)$ and $\phi'(\xi_j x) = \phi'(x)$. We can extend this to a general, smooth transfer function if we restrict the input mode to be uniform, $\xi_j = 1$ for all j. In conclusion, in both the fixed point and limit cycle solutions, the coherent component displays a self-organized criticality which enables the residuals to remain small.

We now consider the transition out of chaos. First, we expect that J_1^c depends on the realizations of $\tilde{\mathbf{J}}$, Equation 16 suggests that J_1 scales as inverse of the overlap between the leading eigenvector and $\boldsymbol{\nu}$. Indeed, we show numerically that the critical value J_1^c for fixed g is negatively correlated with $\left|\boldsymbol{\nu}^T \mathbf{u}^{(1)}\right|$ (Fig 4C). We next ask how J_1^c scales with system size. Since, the typical value of $\left|\boldsymbol{\nu}^T \mathbf{u}^{(1)}\right|$is $O(1)$ we would naively expect that the typical transition might occur for $J_1 \sim O\left(\sqrt{N}\right)$. However, we observe numerically that the fraction of realizations exhibiting chaotic dynamics for a given value of J_1 appears to scale as $\frac{J_1}{N}$ and not as $\frac{J_1}{\sqrt{N}}$ as expected (Fig 4D).

We conclude tentatively that in the limit of large system size chaos persists for all values of J_1. For finite N chaos is lost for some $J_1^c \sim N^\alpha$with $\alpha \in [1/2, 1]$, and the particular J_1^c is highly realization-dependent.

Imprint of fixed point or limit cycle on the chaotic regime

From the previous analysis of the large J_1 regime in which fixed points or limit cycles arise ($J_1 \sim O\left(\sqrt{N}\right)$ at least), we can gain insight into the strongly coherent chaotic dynamics that exists for J_1 large but $O(1)$.

As mentioned above, for large values of J_1 the network dynamics exhibit coherent switching-like activity (Fig 5A top). Furthermore this activity appears to reflect a self-organized criticality as reflected in the speed of the dynamics. We define the speed as the norm of the vector of first time derivatives per neuron: $\sqrt{\frac{1}{N}\sum_i \left(\frac{\mathrm{d}h_i}{\mathrm{d}t}\right)^2}$. Measures such as the speed or its square have been used to find fixed points and slow dynamics in highly non-linear dynamics [26]. As shown in Fig 5A the chaotic trajectories frequently exhibits intervals with low speed. Additionally, the values of $\bar{h}$ come to deviate dramatically from Gaussian and instead become sharply bimodal (Fig 5B).

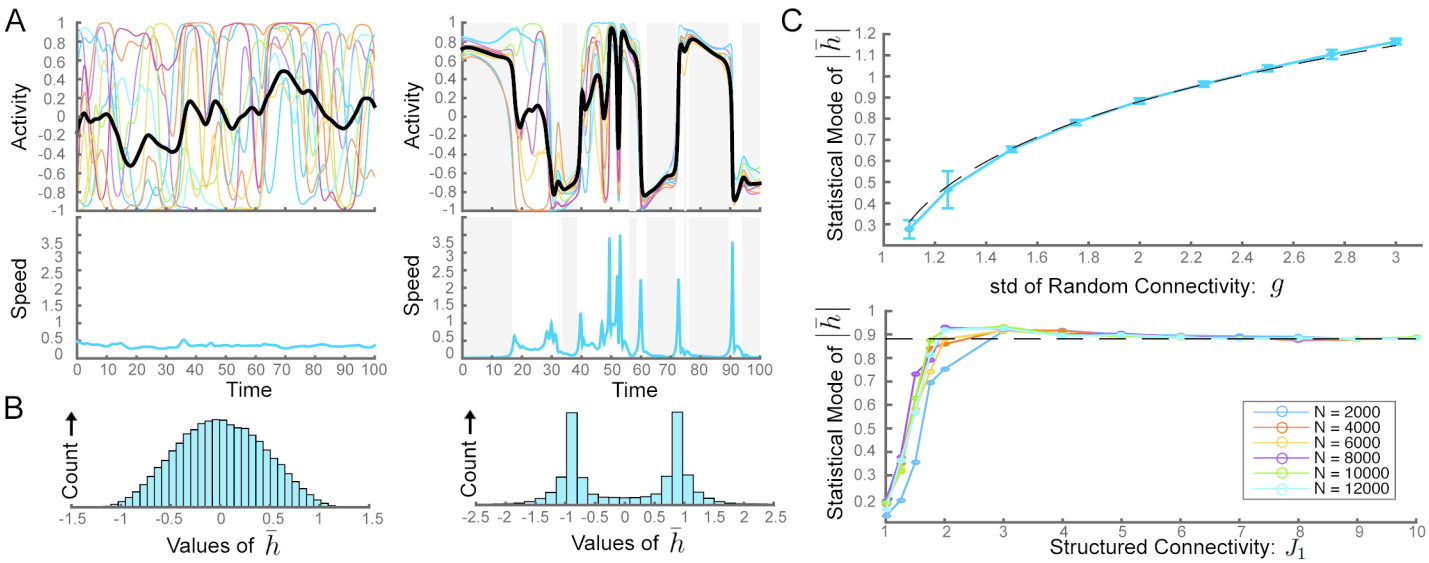

Figure 5. Imprint of Self-Tuned Criticality on the Chaotic Regime. (A) Top: Sample activity of 10 randomly chosen neurons and coherent mode activity, (same as Fig 3). Bottom: Speed of network during same epoch of activity, defined as the per-neuron norm of the rate-of-change vector, i.e. $\sqrt{\frac{1}{N}\sum_i \left(\frac{\mathrm{d}h_i}{\mathrm{d}t}\right)^2}$. For strong structured connectivity, bouts of high and low activity are associated with vanishing speed. **(B)** Histogram of values of the coherent mode current, $\bar{h}(t)$. For strong structured connectivity the histogram is bimodal. **(A)-(B)** Left: $J_1 = 0.8$. Right: $J_1 = 15.8$. **(C)** The statistical mode of $|\bar{h}|$ as a function of g. Dashed line shows the theory prediction from the strong-structure limit, $\bar{h}^* = \sec^{-1}\left(\frac{1}{\sqrt{g}}\right)$. **(D)** Statistical mode of $|\bar{h}|$ as a function of J_1. A crossover occurs very rapidly and independently of N. Dashed line is $\bar{h}^*$. $N = 4000$ and $g = 2$ in all panels where not listed.

We can understand all these phenomena as an imprint of the low-dimensional dynamics of the large J_1 limit on the chaotic regime. We showed above that in both the fixed point and limit cycle solutions the coherent component displays a self-organized criticality which enables the residuals to remain small. This criticality is obtained in both cases at a coherent current with a (fixed or average) value of $\bar{h} = \phi'(1/g)$. We observe numerically that in the chaotic regime the coherent activity intermittently self-organizes near the same critical value yielding slow epochs at both low and high activity. In Fig 5A shaded regions show epochs during which the speed was slower than the slowest dynamics of a network without structured connectivity. We observe that epochs of both low and high activity are associated with very low speed, as well as very high coherence.

This switching between slow states yields a histogram of values of $\bar{h}(t)$ which is highly non-Gaussian and has a bimodal distribution of values with two distinct peaks at $\pm\phi'(1/g)$. We confirm numerically that the most common value of $|\bar{h}|$ as a function of g fits the curve $\phi'(1/g)$ very closely (Fig 5C). Surprisingly, we find that the bimodality of $\bar{h}$ with its peaks at critical values $\pm\phi'(1/g)$ arises already for values of J_1 that are $O(1)$ independent of N (Fig 5C), which appears to reflect a distinct crossover from asynchronous to coherent chaos.

We also observe that in the case of a complex leading eigenvalue of $\tilde{\mathbf{J}}$, the chaotic regime exhibits signatures of

oscillations, which are related to the realization dependent phase of the complex eigenvalue, serving as a precursor of the full limit cycle for larger J_1. This is reflected in the presence of a large second peak in the autocorrelation function (Fig 6A). The height of this second peak grows gradually with J_1 throughout the chaotic regime, with a realization-dependent rate, until a pure limit cycle is reached and the second peak is near 1 (Fig 6B). Furthermore even within the chaotic regime, for most individual realizations the time of the second peak, which reflects the dominant frequency of the fluctuations, is well-predicted by the theoretical prediction for limit cycles: the phase of the leading eigenvalue (see Methods, Fig 6C).

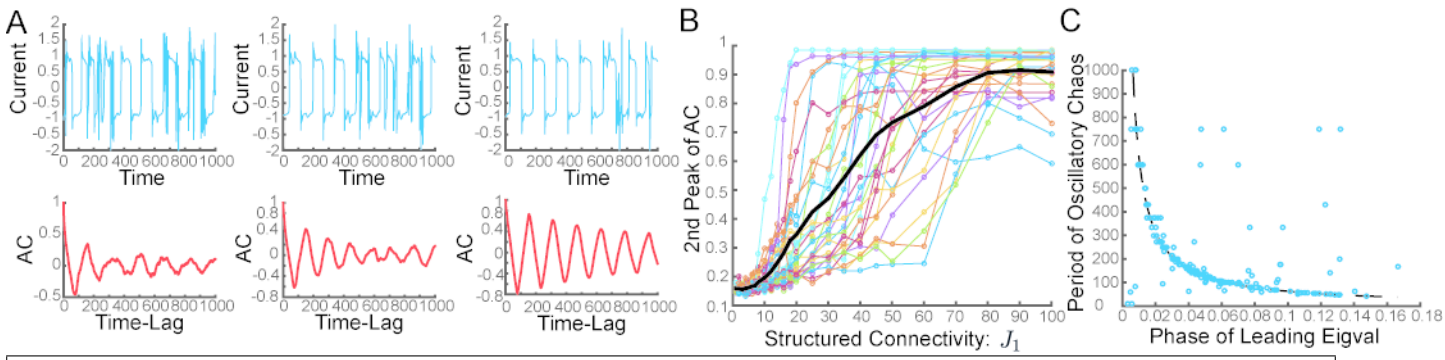

Figure 6. Realization-Dependent Oscillatory Imprint on Chaotic Regime. **(A)** Sample traces (top) and autocorrelation of coherent mode current (bottom) for a connectivity realization with complex eigenvalue for $J_1 = 25, 30, 35$. Dynamics exhibit pronounced oscillatory power and the autocorrelation exhibits a pronounced peak near the same frequency that will dominate the limit cycle for larger J_1. **(B)** Height of second peak of the autocorrelation of the coherent mode input as a function of J_1. Each colored line represents a single connectivity realization, averaged over 10 initial conditions. For many realizations, there is a significant second peak in the autocorrelation over a long range of values of J_1 well before a limit cycle is reached. We display the 30 realizations which had second peak larger than 0.8 for some J_1 within this range. Thick black line shows average over those realizations. **(C)** Observed period of oscillatory chaos vs phase of leading eigenvalue for 181 realizations from which we were able to measure an oscillatory period with chaotic fluctuations (confined to realizations and values of J_1 that yielded second peak of autocorrelation less than 0.8, mean second peak over all realizations: 0.5). Dotted line shows prediction from theory. The bulk of realizations are very well predicted although a notable fraction are not. The median error of prediction was 7.75 (average period: 231, std: 212). $N = 8000$ for all panels.

Likewise, in the case of a real leading eigenvalue, the chaotic dynamics exhibits an imprint of the fixed point. Each of the pair of fixed points (with $\pm\ \bar{h}^*$) break the $h \to -h$ symmetry of the underlying dyanmics, depending on initial condition. Interestingly, we observe that approaching the transition to fixed point, within the chaotic regime, the symmetry is already broken with chaotic trajectories spending more time near one fixed point than the other depending on initial condition (Fig 7A). We measure the asymmetry in a single trial as the absolute value of the time-averaged coherent activity, $\left|\langle \bar{h} \rangle\right|$, and we find that asymmetry grows gradually with J_1 throughout the chaotic regime, and at different rates for different realizations (Fig 7B).

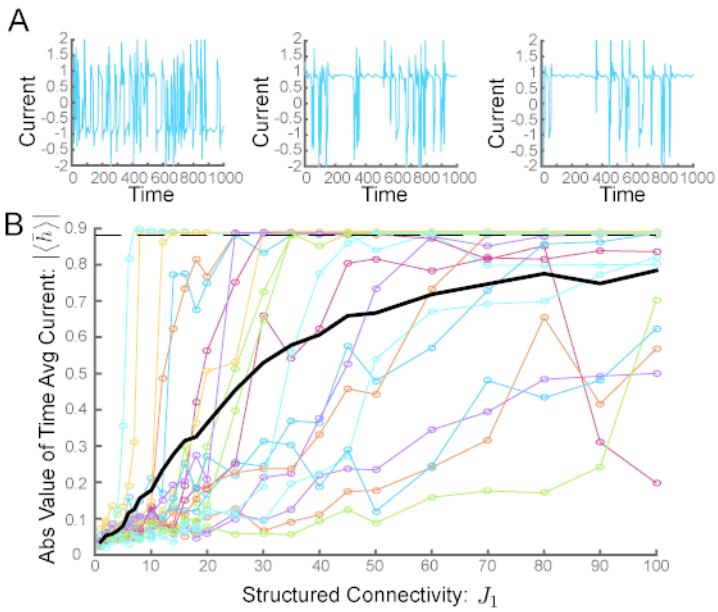

Figure 7. Realization-Dependent Symmetry Breaking in Chaotic Regime. **(A)** Sample traces of coherent mode input current from a connectivity realization with real eigenvalue for $J_1 = 40, 60, 80$ increasing from left to right. Dynamics exhibit pronounced asymmetry. **(B)** Absolute value of the time-average coherent mode input, $|\langle \bar{h} \rangle|$, as a function of J_1. Each colored line represents a single connectivity realization, averaged over 10 initial conditions. For many individual realizations, $|\langle \bar{h} \rangle|$ is significantly non-zero over a long range of values of J_1, while still not arriving at fixed point value (displayed by dashed line). We display the 20 realizations which had $|\langle \bar{h} \rangle| > 0.5$ for some J_1 within this range. Thick black line shows average over those realizations. $N = 8000$ for all panels.

Multiple Modes of Coherence

We generalize our model in order to construct a network with multiple modes of coherent activity. In this extension we take the structural component, $\mathbf{M}$, to be a low-rank matrix comprised of the sum of the outer product of pairs of vectors which are all mutually orthogonal:

$$\mathbf{M} = J_0 \sum_{k=1}^{d} \frac{w_k}{\sqrt{N}} \boldsymbol{\xi}^{(k)} \boldsymbol{\nu}^{(k)^T} \tag{17}$$

where we have introduced a parameter J_0 that controls the overall strength of the structured connectivity, and a set of parameters w_k satisfying $\sum_{k=1}^{d} w_k^2 = 1$ that determine the relative weight of the different modes.

We can extend our schematic representation and think of each row vector $\boldsymbol{\nu}^{(k)^T}$ as a separate output mode connected in a feed-forward-like manner to the input mode, $\boldsymbol{\xi}^{(k)}$, (Fig 8A) and then decompose the dynamics into the residual dynamics identical to the above 4 and the dynamics of the coherent activity along each separate input mode:

$$\frac{\mathrm{d}\bar{h}^{(k)}}{\mathrm{d}t} = -\bar{h}^{(k)} + \frac{J_0 w_k}{\sqrt{N}} \boldsymbol{\nu}^{(k)^T} \boldsymbol{\phi} \tag{18}$$

where each the separate coherent activity is given by $\bar{h}^{(k)} \equiv \frac{1}{N}\sum_j \xi_j^{(k)} h_j$.

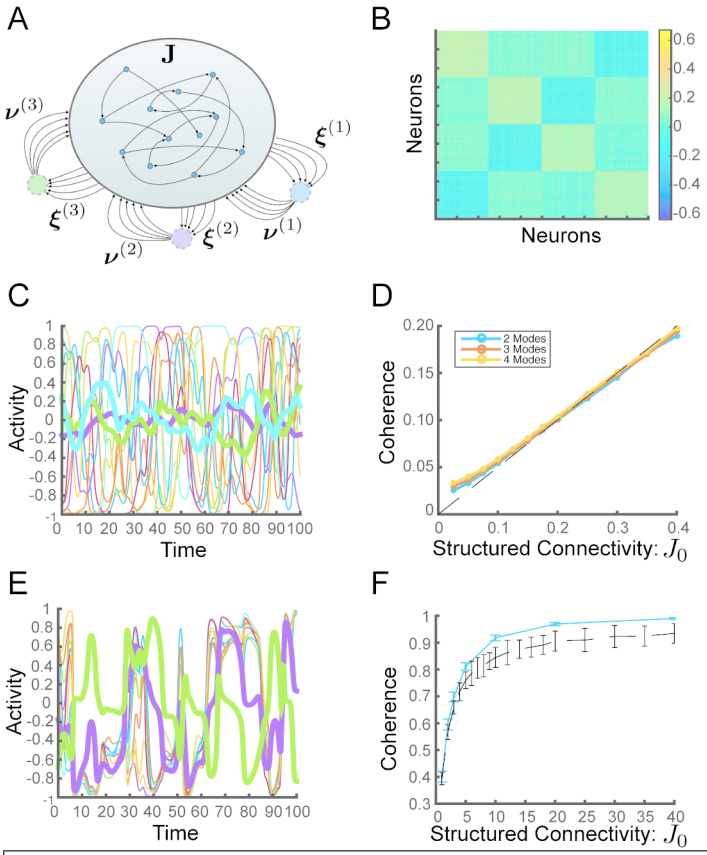

Figure 8. Coherent Chaos Along Multiple Modes. **(A)** Schematic of network with three coherent modes displaying effective output modes, $\boldsymbol{\nu}^{(k)}$, and input modes, $\boldsymbol{\xi}^{(k)}$, each of which are orthogonal to all others. **(B)** Matrix of Pearson correlation coefficients between firing rates, ϕ_i, of pairs pairs of neurons in a network with three coherent modes and $J_1 = 1$. **(C)** Sample activity trace displaying sample single neuron activities and in thicker lines, three coherent mode activities, $\bar{\phi}^{(k)}$. **(D)** Generalized coherence, $\chi^{(k)}$, as a function of $J_1$for 2, 3, 4 modes. Dashed line displays theory. **(E)** Sample activity traces display extreme coherence for two coherent modes. **(F)** Generalized coherence for two coherent modes as a function of J_1 extends to near complete coherence, while chaos persists. Compare network with one coherent mode with dashed line. Bar shows standard deviation over 100 realizations. $N = 2000$ for panels **(B)**, **(C)**, **(E)**. $N = 4096$ for panels **(D)** and **(F)**

The analytical results found above for the regime of mild coherence can be directly extended to the case of multiple modes. In particular, in the limit where $J_0 \ll 1$, the separate coherent modes are independent of each other and driven passively by the residual fluctuations (Fig 8C) such that

$$\bar{\Delta}^{(k)}(\tau) \approx \frac{J_0^2}{g^2} w_k^2 \Delta_\delta(\tau) \tag{19}$$

where $\bar{\Delta}^{(k)}(\tau) = \left\langle \bar{h}^{(k)}(t)\, \bar{h}^{(k)}(t+\tau) \right\rangle$ is the autocorrelation function of the kth coherent mode.

The resulting covariance matrix, $C_{ij} \equiv \langle \phi_i \phi_j \rangle$, has a low-rank structure which is given by the input modes (Fig 8B

). In particular, by Taylor expanding ϕ_i around δh_i:

$$C_{ij} \approx \left(\phi\left(\delta h_i\right) + \phi'\left(\delta h_i\right) \sum_k \bar{h}^{(k)} \xi_i^{(k)} \right) \left(\phi\left(\delta h_j\right) + \phi'\left(\delta h_j\right) \sum_k \bar{h}^{(k)} \xi_j^{(k)} \right) \tag{20}$$

Since the residuals are on average uncorrelated, we find using Eqn 19 that to leading order:

$$\mathbf{C} \approx \left[\phi'\right]_{\mathbf{J}}^2 \Delta_\delta\left(0\right) \frac{J_0^2}{g^2} \sum_{k=1}^{d} w_k^2 \boldsymbol{\xi}^{(k)} \boldsymbol{\xi}^{(k)^T} \tag{21}$$

We generalize our measure of coherence to measure the d-dimensional coherence, or the fraction of total standard deviation which is captured by the d coherent mode directions:

$$\chi^{(d)} \equiv \sqrt{\frac{\sum_{k=1}^{d} \left\langle \left(\bar{h}^{(k)}\right)^2 \right\rangle}{\frac{1}{N}\sum_i \left\langle h_i^2 \right\rangle}} \tag{22}$$

and we find that for $J_k \ll g$ and finite d

$$\chi^{(d)} \approx \frac{J_0}{g} \tag{23}$$

Numerically, this prediction holds well for up to $\frac{J_0}{g} = 0.2$ for at least up to $d = 4$ as we show in Fig 8D, and we expect it to hold for larger d as well.

We note that in the regime of mild coherence, just as in the case of a single coherent mode, we can relax the restrictions on $\boldsymbol{\xi}^{(k)}$ and ϕ. Our results hold for $\boldsymbol{\xi}^{(k)}$ any norm $\sqrt{N}$ vector orthogonal to $\boldsymbol{\nu}^{(j)}$ $\forall j$ and $\boldsymbol{\xi}^{(j)}$ $j \neq k$, and also for ϕ any sigmoidal function.

In addition, we can generalize detailed balance by subtracting the weighted row-average for each input mode such that every $\boldsymbol{\xi}^{(k)}$ will reside in the null space of the new connectivity matrix, $\tilde{\mathbf{J}}^{(d)}$:

$$\tilde{\mathbf{J}}^{(d)} \equiv \mathbf{J} - \mathbf{J} \cdot \frac{1}{N} \sum_{k=1}^{d} \boldsymbol{\xi}^{(k)} \cdot \boldsymbol{\xi}^{(k)^T} \tag{24}$$

For $d > 2$ we this generalized detailed balance does not appear to preserve chaotic fluctuations and instead fixed points or limit cycles appear for $J_0 \sim O\left(1\right)$.

Intriguingly, for $d = 2$ we observe that with generalized detailed balance the chaotic regime persists as the structured connectivity is strengthened and the dynamics become increasingly coherent. The dynamics display switching-like activity in which at any time one of the two coherent modes appears to be near the critical value h^c while the other mode is near zero (Fig 8E). It appears that the generalized coherence approaches 1 while chaos persists (Fig 8F) such that we conjecture that just as in the case of $d = 1$, here too in the large N limit $\chi^{(2)} \to 1$ as $J_0 \to \infty$.

Discussion

Coherent fluctuations are prevalent in cortical activity ranging in spatial scale from shared variability in membrane potential and spiking in local circuits to global signals measured across the scalp via EEG or across voxels via fMRI [31, 22, 1, 10]. Constructing a model that intrinsically generates coherent fluctuations has been a challenge to theorists.

We have studied the generation of coherent chaotic dynamics in recurrent neural networks. Our model consists of rate-based neurons whose recurrent connections include a structured component in addition to random connections. The structured component is a low rank connectivity matrix consisting of outer products between orthogonal pairs of vectors which allow local fluctuations to be summed along an output mode, amplified and projected to an input mode resulting in coherent fluctuations. The orthogonality of input and output mode effectively embeds a feed-forward structure within the recurrent connectivity, thus avoiding feedback of the coherent fluctuations along the input mode.

In the regime where the structured component is weak, the local synaptic currents are effectively uncoupled from the coherent mode activity and their dynamics are similar to that of a random network with no structured component at all. The local fluctuations are summed by the structured component of connectivity to drive the coherent mode, which follows those fluctuations in a passive manner. In this regime a perturbative dynamical mean-field theory following [24, 9] shows that the coherence grows linearly with the ratio of the strength of structured connectivity to the random connectivity. This analysis is easily extended to multiple modes of coherent activity yielding a finite-rank covariance pattern for the coherent fluctuations.

For strong structured component we observe highly coherent chaos in which the dynamics are dominated by a single mode of activity, which undergoes UP-DOWN-like switching activity. We show numerically that as the amplitude of the structured component is increased the dynamics become increasingly coherent. Furthermore, above some critical strength of the structured component, the system converges on a either a fixed point or a limit cycle, depending on individual realization of the random connectivity. The critical amplitude grows with the system size, hence we propose that for all fixed values of structured component, as the network size diverges, coherent chaos persists regardless of the strength of structured component,

Our numerical work suggests that the typical critical strength of structure that yields a transition out of chaos most

likely scales as $J_1 \sim O(N)$ (or at least as $J_1 \sim O\left(\sqrt{N}\right)$), but this requires more work to confirm. On the other hand, the imprint of the fixed points and limit cycles on the chaotic dynamics is apparent already for $J_1 \sim O(1)$. In particular, the Up and Down states we observe in the chaotic dynamics occur at the same values that yield fixed points and up-down limit cycles for very large J_1. The crossover to dynamics of switching-like activity between these state occurs for $J_1 \sim O(1)$, independent of network size.

In the regime of weak structured connectivity some of the assumptions of our model can be loosened. In this regime we need not require the input mode be binary but rather a any general pair of orthogonal vectors can be used. This is in fact what we have done numerically in the section on multiple modes. Moreover we can loosen the restriction on orthogonality: a random pair of vectors can serve as input and output mode without qualitative impact on the dynamics presented here because the contribution of the realization-dependent overlap in this regime will be negligible relative to the typical contribution from the random component.

It should be stressed that the regime of strong structured connectivity, on the other hand, requires the network be finely-tuned to a high degree. The orthogonality of the input and output modes is not enough in order to achieve highly coherent chaos because of interactions between the random and structured components of connectivity. We therefore constrain the random component to satisfy detailed balance by ensuring that the input mode of the structured connectivity be in the null-space of the random component of connectivity.

In addition to detailed balance, the high coherence regime depends on the choice of the single-neuron transfer function and input-mode vector. Our particular choice of hyperbolic tangent, which has been inherited from statistical physics, is an odd function: $\phi(\xi_i x) = \xi_i \phi(x)$ and $\phi'(\xi_i x) = \phi'(x)$ for $\xi_i = \pm 1$. The first equality acts in concert with the detailed balance to filter out the coherent-mode activity. The second equality guarantees that the coherent mode input acts as a dynamic-gain on the dynamics of the residuals in a uniform way. As mentioned in the main text, we can loosen the requirement of an odd transfer function at the cost of requiring a uniform input mode, $\xi_i = 1 \, \forall i$. The theory developed here predicts coherent fluctuations that switch between slow points where the slope of the transfer function is $1/g$, and that is what we have observed numerically (data not shown).

In this case of a uniform input mode the model can be constructed as a excitation-inhibition network, for example with half the neurons defined as excitatory by setting $\nu_i = 1$ and the other half defined as inhibitory via $\nu_i = -1$ (or a larger inhibitory value to compensate for a smaller fraction of inhibitory neurons). From this perspective the coherent fluctuations can be understood within the framework dynamic E-I balance [30]. In this case the pair of balance equations are degenerate and require simply that the mean excitatory population rate nearly equal the inhibitory rate, but otherwise leave the overall mean rate unconstrained. Local residual fluctuations yield only small

differences is mean population rates, thus leaving the balance satisfied, but these small differences drive significant coherent fluctuations because of the strong balanced connectivity . We note that excitation-inhibition networks in the literature have sometimes been constructed in this manner. As we have shown here, such choices have dramatic impact on the dynamics and the results should not be assumed to be generalizable.

In parallel to our study a pre-print has been published which explores a very similar model[8]. The authors observe a similar phenomenon numerically and write similar mean-field equations. Whereas we have focused on analytical solutions to these equations in the limit of both weak and strong structured connectivity, the authors develop an iterative approach to numerically solve the equations. They restrict their study to the case of a single orthogonal E-I structured component, and they appear to come to different conclusions about the realization-dependence and the role of detailed balance.

As mentioned in the main text and introduction, a previous study also explored the case of a single orthogonal E-I structured component[6]. They derived the fixed point and limit cycle solutions which we reviewed here, but did not focus on the chaotic regime and they did not discuss the role of network size in the transition out of chaos. Our focus here was on the chaotic regime, both the emergence of coherence for small structured connectivity and the imprint of the non-chaotic regime on the chaotic dynamics for moderate structured connectivity.

A separate pre-print has claimed to observe coherent activity in excitation-inhibition networks of spiking neurons [29]. A study of the dynamics of spiking neurons is beyond the scope of our work, although we would conjecture that coherent activity would arise with orthogonal, rank-one E-I structure in the case of spiking as well.

Previous work has shown how shared inputs from external drive can drive correlated fluctuations in excitation-inhibition networks [5, 20]. In our current work, in the context of rate neurons, we show that such correlated fluctuations can be generated internally by a recurrent network without external drive. In order to avoid either saturation or pure oscillations the coherent activity mode must not drive itself through a feedback loop. In order to achieve this it is necessary that the structured component embed an effectively-feedforward projection between a pair of orthogonal modes. In parallel, Darshan et al [4] have developed a theory for internally generated correlations in excitation-inhibition networks of binary units. The underlying principle is similar: the recurrent connectivity embeds a feedforward-like structure in which a pair of orthogonal modes are connected.

We note that the structured component of connectivity is non-normal. The dynamics of non-normal matrices have drawn a fair amount of interest with suggested functional impact on working memory [**?**, 7] and amplification [12]. Non-normal matrices embed feed-forward structure within recurrent connectivity, and the resulting dynamics even

in a linear system are not fully determined by the eigenspectrum but depend on the structure of the corresponding eigenvectors. Feed-forward structure can be revealed by the Schur decomposition and the extent of feedforwardness can be measured as the fraction of total power (sum-of-squares) that is off the diagonal in the Schur decomposition. The structured component in our model can be rightly considered an extreme case of non-normality as it has only zero eigenvalues and therefore all its power is in the off-diagonal. The chaotic dynamics studied here are a distinctly non-linear effect and therefore the Schur decomposition alone gives little insight. We have instead focused our analytical work on the two regimes of weak and strong structured connectivity.

Rate model dynamics with a rank-one structured component have been studied in depth recently, but these have not focused on the particular case of the outer product of orthogonal vectors [19, 11]. These works also differed in that the strength of the structured connectivity was scaled as $1/N$. This scaling is similar to our limit of weak structured connectivity, $J_1 \ll 1$, and guarantees that dynamic mean-field theory holds in the limit of large system size.

It has been previously observed [17] and then proven [27] that adding an orthogonal outer-product to a random matrix generates realization-dependent outliers in the eigenspectrum, and furthermore that these outliers are be removed by detailed balance. It has been previously observed that performing such a subtraction has significant impact on the resulting dynamics [6, 25]. Yet the relationship between the change in eigenspectrum and the dynamics has not been made clear beyond the basic observations regarding the stability of a fixed-point at zero. Here we suggest that the impact of detailed balance on the chaotic dynamics is not directly related to the eigenspectrum but that this adjustment should be thought of as effectively subtracting the coherent-mode activity from each individual neuron, thus decorrelating the residual synaptic current. We show that detailed balance preserves self-averaging for moderate values of structured connectivity and that it is crucial for the emergence of highly coherent dynamics.

In conclusion we have presented a simple model which generates coherent chaos in which macroscopic fluctuations emerge through the interplay of random connectivity and a structured component that embeds a feedforward connection from an output mode to an orthogonal input mode.

Methods

Perturbative Dynamic Mean-Field Theory

We derive the dynamic mean-field equations in the limit of small J_1 using a perturbative approach. Extending previous results, we assume the residual currents δh_i fluctuate as independent Gaussian processes, and then

autocorrelation of the residuals, $\Delta_\delta(\tau) = \langle \delta h_i(t)\, \delta h_i(t+\tau)\rangle$ is given by the self-consistency equation:

$$\left(1 - \frac{\partial^2}{\partial \tau^2}\right) \Delta_\delta(\tau) = g^2 C(\tau) \tag{25}$$

where $C(\tau) \equiv \langle \delta\phi_i(t)\, \delta\phi_i(t+\tau)\rangle$ with $\delta\phi_i \equiv \phi_i - \xi_i \bar{\phi}$.

This can be written $C(\tau) = \langle \phi_i(t)\, \phi_i(t+\tau)\rangle - \left\langle \bar{\phi}(t)\, \bar{\phi}(t+\tau)\right\rangle$.

For $J_1 \ll 1$ we assume that $\left|\bar{h}\right|$, we have $\phi_i = \phi\left(\delta h_i + \xi_i \bar{h}\right) \approx \phi(\delta h_i) + \xi_i \phi'(\delta h_i)\, \bar{h}$. This yields $\left[\bar{\phi}^2\right] \sim O\left(\frac{1}{N}\right)$ so that $C(\tau) \approx \langle \phi_i(t)\, \phi_i(t+\tau)\rangle$ to zeroth order. And additionally using $\phi_i(t) \approx \phi(\delta h_i)$ allows us to follow previous work and write to zeroth order

$$C(\tau) \approx \int_{-\infty}^{\infty} Dz \left(\int_{-\infty}^{\infty} Dx\, \phi\left(\sqrt{\Delta_\delta(0) - \Delta_\delta(\tau)}\, x + \sqrt{\Delta_\delta(\tau)}\, z\right)\right)^2 \tag{26}$$

Thus Eqn 25 reduces to leading order to the equation for a random network without structured component[24]. Thus $\Delta_\delta(\tau) \approx \Delta_0(\tau)$, where $\Delta_0(\tau)$ is the autocorrelation when $J_1 = 0$

Therefore the δh_j are nearly independent and we can treat the sum $\frac{1}{\sqrt{N}} \sum_j \nu_j \phi_j$ as a Gaussian process which itself has autocorrelation approximately given by $C(\tau)$. This yields an equation for the autocorrelation of $\bar{h}$, $\bar{\Delta}(\tau) \equiv \left\langle \bar{h}(t)\, \bar{h}(t+\tau)\right\rangle$:

$$\left(1 - \frac{\partial^2}{\partial \tau^2}\right) \bar{\Delta}(\tau) = J_1^2 C(\tau) \tag{27}$$

This equation tells us that for $J_1 \ll 1$ fluctuations in the coherent input are driven passively by the random source which is generated self-consistently by the residual fluctuations, and that to first order the resulting coherent autocorrelation is

$$\bar{\Delta}(\tau) \approx \frac{J_1^2}{g^2} \Delta_0(\tau) \tag{28}$$

Analysis of Fixed Points and Limit Cycles

In the limit of large J_1 we assume $\delta h_i \ll 1$, and approximate $\phi_j \approx \phi\left(\xi_j \bar{h}\right) + \phi'\left(\bar{h}\right) \delta h_j$, where we have made use of the symmetry of the transfer function and the binary restriction on ξ_j. This yields dynamical equations:

$$\frac{\mathrm{d}\delta \mathbf{h}}{\mathrm{d}t} = -\delta \mathbf{h} + \phi'\left(\bar{h}\right) \tilde{\mathbf{J}} \delta \mathbf{h} \tag{29}$$

$$\frac{\mathrm{d}\bar{h}}{\mathrm{d}t} = -\bar{h} + \frac{J_1}{\sqrt{N}} \phi'\left(\bar{h}\right) \boldsymbol{\nu}^T \delta \mathbf{h} \tag{30}$$

Note that the leading term of the linearization, $\phi\left(\xi_i \bar{h}\right) = \xi_i \phi\left(\bar{h}\right)$ has fallen from both sums. This reflects the important role of the orthogonality of $\boldsymbol{\nu}$ and $\boldsymbol{\xi}$ on the one hand, and the subtraction we made to the random

connectivity, both of which ensure that the coherent mode does not drive a feedback loop. Crucially though, this depends on the symmetry of the transfer function, ϕ, and the assumption that $\xi_i = \pm 1$. For a general transfer function this linearization holds only in the case of uniform $\boldsymbol{\xi}$.

In this regime $\bar{h}$ acts as a dynamic gain on the local synaptic currents through $\phi'\left(\bar{h}\right)$. The equation for the residual currents is linear and therefore their dynamics can be decomposed in the eigenbasis of $\tilde{\mathbf{J}}$ which we write as $\left\{\mathbf{u}^{(i)}\right\}_{i=1}^{N}$ with $\tilde{\mathbf{J}} \cdot \mathbf{u}^{(i)} = \lambda_i \mathbf{u}^{(i)}$. Writing the vector of residual current as $\delta\mathbf{h} = \sum_i c_i \mathbf{u}^{(i)}$ yields dynamics

$$\frac{\mathrm{d}c_i}{\mathrm{d}t} = -c_i + \phi'\left(\bar{h}\right)\lambda_i c_i \tag{31}$$

the the only (marginally) stable, non-zero fixed point is achieved with $c_1 \neq 0$ and $c_i = 0$ for all $i > 1$. And the fixed-point equation is

$$c_1^*\left(1 - \phi'\left(\bar{h}\right)\lambda_1\right) = 0 \tag{32}$$

This fixed point only exists if λ_1 is real, and yields a fixed-point requirement for $\bar{h}^*$:

$$\bar{h}^* = \phi'^{-1}\left(\frac{1}{\lambda_1}\right) \approx \phi'^{-1}\left(\frac{1}{g}\right) \tag{33}$$

In order to close the loop we turn to the fixed point equation for the coherent dynamcis:

$$\bar{h}^* = \frac{J_1}{\sqrt{N}}\phi'\left(\bar{h}\right)\boldsymbol{\nu}^T\delta\mathbf{h}^* \tag{34}$$

which in turn using $\delta\mathbf{h}^* = c_1\mathbf{u}^{(1)}$ yields a solution for c_1: $c^* = \frac{\bar{h}^*\lambda_1}{\bar{J}_1\left(\boldsymbol{\nu}^T\mathbf{u}^{(1)}\right)}$, as reported in [6].

If λ_1 is complex there is no fixed-point but rather a limit-cycle solution to the dynamics of the complex-valued c_1 exists, assuming $c_i = 0$ for all $i > 0$. Assuming $\bar{h}\left(t\right)$ is periodic with period T, $c_1\left(t\right)$ is given by

$$c_1\left(t\right) = c_1\left(0\right)\exp\left(-t + \lambda_1\Phi\left(t\right)\right) \tag{35}$$

for $t \leq T$, where $\Phi\left(t\right) = \int_0^t \mathrm{d}s\,\phi'\left(s\right)$. A limit-cycle in phase with $\bar{h}\left(t\right)$ requires $c_1\left(T\right) = c_1\left(0\right)$ and this requires the $\mathrm{Im}\left[\lambda_1\Phi\left(T\right)\right]$ equal 2π. This means that the average value of ϕ' over a period must be the critical value $\langle\phi'\rangle = \frac{\Phi(T)}{2\pi} = \frac{1}{\lambda_1} \approx \frac{1}{g}$.

Furthermore we can derive the period of the limit cycle by noting that in order for $c_1\left(T\right) = c_1\left(0\right)$ we must have $\mathrm{Re}\left[\lambda_1\Phi\left(T\right)\right] = T$. Combining this with the previous requirements yields an expression for the period (as reported in [6]):

$$T = 2\pi\frac{\mathrm{Re}\lambda_1}{\mathrm{Im}\lambda_1} \tag{36}$$

Simulations confirm that a projection of the full synaptic current dynamics into the coherent mode and the leading eigenvector plane (consisting of real and imaginary parts of $\mathbf{u}^{(1)}$) accounts for well over 0.99 of the total variance. Even restricting ourselves to the variance of the residuals, δh_i, we find that 0.98 of the variance is restricted to the leading eigenvector plane (Fig S3).

For $N = 4000$ we simulate 219 realizations of random connectivity with complex leading eigenvalue and find that for sufficiently large $\tilde{J}_1$ all but one of these realizations yield highly oscillatory dynamics with period predicted nearly perfectly by theory (Fig S3).

We note that in the limit of large N we expect that the typical size of the imaginary component of the leading eigenvalue, λ_1, shrinks such that the typical period grows. These longer period oscillations are characterized by square-wave-like shape in which the dynamics of the coherent component slows around the critical value $\bar{h}^c = \phi^{-1}\left(\frac{1}{\mathrm{Re}\lambda_1}\right)$, which is identical to the fixed-point value of $\bar{h}$ when λ_1 is real. (Fig S3)

Lyapunov Exponent, Limit Cycles, and Fixed Points

In order to calculate the largest Lyapunov exponent, we begin with a point $\mathbf{h}_0$ along the trajectory of the dynamics and we solve concurrently for the dynamics of the trajectory, $\mathbf{h}(t)$ with $\mathbf{h}(0) = \mathbf{h}_0$, and for a randomly chosen perturbation, $\boldsymbol{\eta}(t)$. The trajectory $\mathbf{h}(t)$ yields the Jacobian matrix for each point along the trajectory:

$$\mathcal{J}_{ij}(t) = -1 + J_{ij}\phi'(h_j(t)) \tag{37}$$

We choose a random unit-norm vector $\boldsymbol{\eta}(0) = \boldsymbol{\eta}_0$ and iterate the linearized dynamics of the perturbation:

$$\frac{\mathrm{d}\boldsymbol{\eta}}{\mathrm{d}t} = \boldsymbol{\mathcal{J}}\boldsymbol{\eta} \tag{38}$$

The largest Lyapunov exponent is given by

$$\lim_{t\to\infty} \frac{1}{t} \log \|\boldsymbol{\eta}(t)\| \tag{39}$$

In practice we iterate 38 until $t = 5000$, that is, 5000 times the intrinsic time-scale of the dynamics, and we renormalize $\boldsymbol{\eta}(t)$ at intervals of $t = 100n$ for $n = \{1, 2, ..., 50\}$.

We classify fixed points numerically by a threshold on the fluctuations of the coherent input: $\mathrm{std}\left(\bar{h}(t)\right) \leq 5\mathrm{x}10^{-4}$.

We classify limit cycles by a threshold on the second peak of the normalized coherent autocorrelation: $q_{peak} \geq 0.9$.

We confirm that all of the trials with negative Lyapunov exponent were categorized as either fixed points or limit cycles. A small fraction of trials classified as limit cycles had positive Lyapunov exponents but with the largest one 0.0043.

Acknowledgements

We thank Rainer Engelken for advice on numerically calculating Lyapunov exponents. This work was funded by the Gatsby Charitable Foundation and the NIH.

References

[1] Peter Achermann, Thomas Rusterholz, Roland Dürr, Thomas König, and Leila Tarokh. Global field synchronization reveals rapid eye movement sleep as most synchronized brain state in the human EEG. *Royal Society Open Science*, 3(10):160201, 2016.

[2] Anne K. Churchland, R. Kiani, R. Chaudhuri, Xiao Jing Wang, Alexandre Pouget, and M. N. Shadlen. Variance as a Signature of Neural Computations during Decision Making. *Neuron*, 69(4):818–831, 2011.

[3] Marlene R. Cohen and John H.R. Maunsell. Attention improves performance primarily by reducing interneuronal correlations. *Nature Neuroscience*, 12(12):1594–1600, 2009.

[4] Ran Darshan, Carl van Vreeswijk, and David Hansel. How strong are correlations in strongly recurrent neuronal networks? *arXiv*, (1):1–22, 2018.

[5] Ran Darshan, William E. Wood, Susan Peters, Arthur Leblois, and David Hansel. A canonical neural mechanism for behavioral variability. *Nature Communications*, 8(May):15415, 2017.

[6] Luis Carlos García Del Molino, Khashayar Pakdaman, Jonathan Touboul, and Gilles Wainrib. Synchronization in random balanced networks. *Physical Review E - Statistical, Nonlinear, and Soft Matter Physics*, 88(4):1–5, 2013.

[7] Mark S Goldman. Memory without Feedback in a Neural Network. *Neuron*, 61(4):621–634, 2009.

[8] Takashi Hayakawa and Tomoki Fukai. Spontaneous and stimulus-induced coherent states of dynamically balanced neuronal networks. *arXiv*, (1):1–36, 2018.

[9] Jonathan Kadmon and Haim Sompolinsky. Transition to chaos in random neuronal networks. *Physical Review X*, 5(4):1–28, 2015.

[10] Thomas T. Liu, Alican Nalci, and Maryam Falahpour. The global signal in fMRI: Nuisance or Information? *NeuroImage*, 150(February):213–229, 2017.

[11] Francesca Mastrogiuseppe and Srdjan Ostojic. Linking connectivity, dynamics and computations in recurrent neural networks. *arXiv*, pages 1–70, 2017.

[12] Brendan K Murphy and Kenneth D Miller. Balanced Amplification: A New Mechanism of Selective Amplification of Neural Activity Patterns. *Neuron*, 61(4):635–648, 2009.

[13] Kevin Murphy and Michael D. Fox. Towards a consensus regarding global signal regression for resting state functional connectivity MRI. *NeuroImage*, 154:169–173, 2017.

[14] P L Nunez, R B Silberstein, M R Carpentar, R Srinivisan andR.S. Wijesinghe, D M Tucker, P J Cadusch, and X Wu. EEG coherency II: Experimental comparison of multiple measures. *Electroenceaphlogr Clin Neurophysiol*, 110:469, 1999.

[15] M. Okun, P. Yger, S. L. Marguet, F. Gerard-Mercier, A. Benucci, S. Katzner, L. Busse, M. Carandini, and K. D. Harris. Population Rate Dynamics and Multineuron Firing Patterns in Sensory Cortex. *Journal of Neuroscience*, 32(48):17108–17119, 2012.

[16] Michael Okun, Nicholas a. Steinmetz, Lee Cossell, M. Florencia Iacaruso, Ho Ko, Péter Barthó, Tirin Moore, Sonja B. Hofer, Thomas D Mrsic-Flogel, Matteo Carandini, and Kenneth D Harris. Diverse coupling of neurons to populations in sensory cortex. *Nature*, 2015.

[17] Kanaka Rajan and L F Abbott. Eigenvalue Spectra of Random Matrices for Neural Networks. *Physical Review Letters*, 97(18):188104, nov 2006.

[18] Alfonso Renart, Jaime De Rocha, Peter Bartho, Liad Hollender, Néstor Parga, Alex Reyes, and Kenneth D Harris. The Asynchronous State in Cortical Circuits. *Science (New York, N.Y.)*, 327(January):587–590, 2010.

[19] Alexander Rivkind and Omri Barak. Local Dynamics in Trained Recurrent Neural Networks. *Physical Review Letters*, 118(25):1–5, 2017.

[20] Robert Rosenbaum, Matthew A Smith, Adam Kohn, Jonathan E Rubin, and Brent Doiron. The spatial structure of correlated neuronal variability. *Nature Neuroscience*, 20(October):1–35, 2016.

[21] M. L. Scholvinck, A. Maier, F. Q. Ye, J. H. Duyn, and D. A. Leopold. Neural basis of global resting-state fMRI activity. *Proceedings of the National Academy of Sciences*, 107(22):10238–10243, 2010.

[22] Matthew a Smith and Adam Kohn. Spatial and temporal scales of neuronal correlation in primary visual cortex. *The Journal of neuroscience : the official journal of the Society for Neuroscience*, 28(48):12591–603, nov 2008.

[23] W R Softky and C Koch. The highly irregular firing of cortical cells is inconsistent with temporal integration of random EPSPs. *The Journal of neuroscience : the official journal of the Society for Neuroscience*, 13(1):334–50, jan 1993.

[24] Haim Sompolinsky, A. Crisanti, and H. J. Sommers. Chaos in random neural networks. *Physical Review ...*, 61(3):259–262, 1988.

[25] Merav Stern and L F Abbott. Dynamics of rate-model networks with seperate excitatory and inhibitory populations. *The annual meeting of the Society for Neuroscience*, 2016.

[26] David Sussillo and Omri Barak. Opening the black box: low-dimensional dynamics in high-dimensional recurrent neural networks. *Neural computation*, 25(3):626–49, mar 2013.

[27] Terence Tao. Outliers in the spectrum of iid matrices with bounded rank perturbations. *Probability Theory and Related Fields*, 155(1-2):231–263, 2013.

[28] B Tirozzi and M Tsodyks. Chaos in highly diluted neural networks. *EPL (Europhysics Letters)*, 14(8):727–732, 1991.

[29] Ekkehard Ullner, Antonio Politi, and Alessandro Torcini. Ubiquity of collective irregular dynamics in balanced networks of spiking neurons. *arXiv*, pages 1–5, 2017.

[30] Carl van Vreeswijk and Haim Sompolinsky. Chaotic balanced state in a model of cortical circuits. *Neural computation*, 10(6):1321–71, aug 1998.

[31] Maxim Volgushev, Sylvain Chauvette, and Igor Timofeev. Long-range correlation of the membrane potential in neocortical neurons during slow oscillation. *Progress in Brain Research*, 193:181–199, 2011.

Supplementary Figure 1

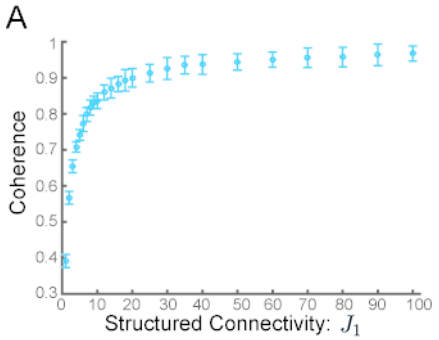

Figure S1 (see Fig 3). Near Perfect Coherence as Strength of Structured Connectivity is Increased. (A) Plot of coherence, χ, vs strength of structured connectivity, J_1, for networks of size $N = 16000$. Dots display average over realizations, bars display standard deviation. Only chaotic realizations included (those not found to be at a fixed point or a limit cycle - see methods). More than 20 realizations per value of J_1. For $J_1 = 100$, 22 out of 30 realizations were chaotic and the average coherence was 0.963.

Supplementary Figure 2

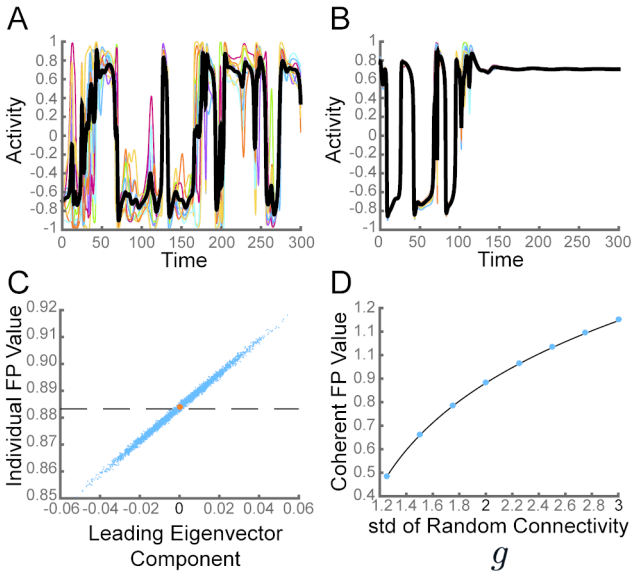

Figure S2 (see Fig 4). Real Leading Eigenvalues Yield Fixed Points. (A) Sample chaotic dynamics for $J_1 = 0.1$. **(B)** Sample dynamics of same connectivity realization as in (A) but with $J_1 = 1$. **(C)** Scatterplot of all individual local-fields at fixed point, h_i^*, plotted against individual components of the leading eigenvector, u_i^1. Red dot is value of coherent mode at FP. Black dashed line is FP value predicted from theory. **(D)** Value of coherent mode of local-field at FP, y^*, as a function of the standard deviation of the random connectivity, g. Black line is prediction from theory: $y^* = \text{sech}^{-1}\left(\frac{1}{\sqrt{g}}\right)$. $N = 4000$.

1 Supplementary Figure 3

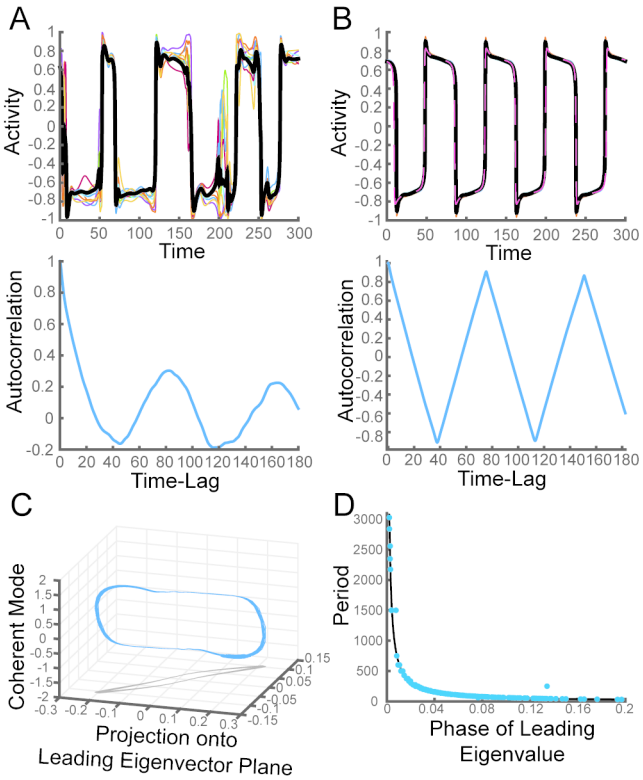

Figure S3 (see Fig 4). Complex Leading Eigenvalues Yield Limit Cycles. (A) Top: Sample chaotic dynamics for $J_1 = 0.25$. Bottom: Autocorrelation of coherent mode of local-field shows oscillatory ringing. **(B)** Same connectivity realization as (A) but with $J_1 = 2$. Dashed pink line in top panel is prediction from solving the three-dimensional dynamics. Autocorrelation shows near-perfect oscillations. **(C)** Projection of the full local-field dynamics of (B) onto coherent mode and the real and imaginary parts of the leading eigenvector. These three dimensions account for more than 0.99 of the total variance. Gray projection onto the leading eigenvector plane accounts for 0.98 of the variance of the residual local fields. **(D)** Scatterplot of period of oscillations plotted against the relative imaginary part of the leading eigenvalue, $e_1 = \frac{\mathrm{Re}\lambda_1}{\mathrm{Im}\lambda_1}$, for 219 different realizations of the random connectivity. Black line shows prediction from theory, $T = \frac{2\pi}{\mathrm{Im}[e_1]}$.